www.springer.com/41230
https://doi.org/10.1007/s41230-022-1036-z

High-strength aluminum alloys hollow billet prepared by two-phase zone continuous casting

Yao-hua Yang[1, 2, 3, 4], *Xue-feng Liu[1, 2, 3], and Wang-zhang Chen[2, 3]

1. Beijing Advanced Innovation Center for Materials Genome Engineering, University of Science and Technology Beijing, Beijing 100083, China

2. Beijing Laboratory of Metallic Materials and Processing for Modern Transportation, University of Science and Technology Beijing, Beijing 100083, China

3. Key Laboratory for Advanced Materials Processing of Ministry of Education, University of Science and Technology Beijing, Beijing 100083, China

4. Shunde Graduate School, University of Science and Technology Beijing, Foshan 528399, Guangdong, China

Abstract: The two-phase zone continuous casting (TZCC) technique was used to continuously cast high-strength aluminum alloy hollow billets, and a verified 3D model of TZCC was used to simulate the flow and temperature fields at casting speeds of 2–6 mm·min^{-1}. Hollow billets under the same conditions were prepared, and their macro/microstructures were analyzed by an optical microscope and a scanning electron microscope. During the TZCC process, a circular fluid flow appears in front of the mushy zone, and the induction heated stepped mold and convective heat transfer result in a curved solidification front with depressed region near the inner wall and a vertical temperature gradient. The deflection of the solidification front decreases and the average cooling rate in the mushy zone increases with increasing casting speed. Experimental results for a 2D12 alloy show that hot tearing periodically appears in the hollow billet accompanied by macrosegregation near the inner wall at casting speeds of 2 and 4 mm·min^{-1}, while macroscopic defects of hot tearing and macrosegregation weaken and the average size of columnar crystals in the hollow billets decreases with further increasing casting speed. 2D12 aluminum alloy hollow billets with no macroscopic defects, the finest columnar crystals, and excellent mechanical properties were prepared by TZCC at a casting speed of 6 mm·min^{-1}, which is beneficial for the further plastic forming process.

Keywords: two-phase zone continuous casting; high-strength aluminum alloy; hollow billet; fluid flow; heat transfer; columnar crystals

CLC numbers: TG146.21 **Document code:** A **Article ID:** 1672-6421(2022)03-253-10

1 Introduction

High-strength and lightweight metal tubes are widely used in the aerospace, transportation, electric power system, and petrochemical industries [1, 2]. Plastic forming processes are usually used to fabricate metal tubes for improving dimensional accuracy and mechanical properties. A hollow billet is required before the plastic forming processes, which could be prepared by piercing of billets or liquid forming. Li et al. [3] and Zhang et al. [4] stated that inhomogeneous deformation occurred during cold pilgering and rotary tube piercing processes, which affected the formability and performance of the tubes. The hollow billets prepared by liquid forming, including centrifugal casting, spray forming and continuous casting, avoid the severe uneven deformation during the piercing process and have the advantages of low energy consumption, low cost, simple production procedures, and excellent performance. The insufficient deposit quality in terms of porosity and bonding to the substrate limits the application of the spray forming method [5]. Fu et al. [6] suggested that centrifugal casting had a strong tendency to segregate and caused nonuniformity of hardness and tensile strength in hollow cast-iron bars. Researchers have found that the continuous casting technique is the most promising method for preparing hollow billets with excellent performance and high efficiency. Hollow cast-iron bars with no segregation, compact microstructures and finer grains were prepared by vertical continuous casting [7].

However, high-strength aluminum alloys always have many alloying elements and a wide solidification

***Xue-feng Liu**

Born in 1970, Professor. Mainly engaged in the research of new technology and theory of high performance and difficult-to-machine metal materials in short process with high efficiency. He is the authored or coauthored of nearly 200 peer-reviewed journal papers, and authorizes more than 100 invention patents.

E-mail: liuxuefengbj@163.com

Received: 2021-02-21; Accepted: 2021-12-13

interval, which easily form macrosegregation and hot tearing during traditional continuous casting processes [8-10]. During the continuous casting of high-strength aluminum alloys by the direct-chill casting method, negative segregation can be observed in the centerline and subsurface, whereas positive segregation appears in the surface, and somewhat underestimated positive segregation in the middle radius [11]. Moreover, hot tearing is the main macroscopic defect during direct-chill casting high-strength aluminum alloys [12, 13]. Mathier et al. [14] pointed out that increasing the casting speed accelerated the occurrence of hot tearing in the center of the billet where high stress and strains occurred. Suyitno et al. [15] found that the maximum hot tearing susceptibility corresponded to the deepest sump during direct-chill casting, which was formed due to the intensive cooling of the water-cooled mold. As a consequence, the characteristics of heat and solute transfer in the mushy zone during continuous casting of high-strength aluminum alloys (with a wide solidification interval) are the key factors that affect the performance of the hollow billets.

To solve the problems of macrosegregation and hot tearing when continuously casting alloys that have a wide solidification interval, Liu et al. [16] proposed the two-phase zone continuous casting (TZCC) technique. During the TZCC process, the mold is induction heated, and the temperature is controlled within the solidification interval of the alloy. The induction heated mold decreases the temperature difference between the mold and melt, which is beneficial for controlling the radial heat transfer and vertical temperature gradient during solidification. Yang et al. [17] proved that a stepped diameter mold could improve the uniformity of the electromagnetic field, and enhance the temperature gradient in the melt during the TZCC process, which is beneficial to control the macrosegregation and hot tearing during solidification.

In this study, the TZCC technique was applied to prepare high-strength aluminum alloy hollow billets to eliminate the macroscopic defects and improve their performance. A 2D12 aluminum alloy was selected as an example, and a stepped diameter mold with a fixed core rod was designed. Based on a verified 3D TZCC model, the temperature field and flow field under different casting speeds were calculated. Hollow billets were prepared under identical conditions, and the characteristics of the hollow billets were investigated.

2 Numerical simulation and experimental description

2.1 Geometry definition

Figures 1(a) and (b) show the overall structure of the TZCC equipment. A simplified 3D model of the TZCC equipment with continuous melting and casting was established, as shown in Fig. 1(c). The mesh was generated using ANSYS (distributed by ANSYS USTB), as displayed in Fig. 1(d). The stepped diameter mold with an integrated flow channel was designed and built, as displayed in Figs. 1(d–f). The upper part with a larger inner cavity is the flow channel for melt supply, while the lower part with a smaller inner cavity is the two-phase zone mold for solidification control. The temperature of the two-phase zone mold was controlled by induction heating coils within the solidification interval of the 2D12 aluminum alloy during experiments. The fixed graphite core rod in the mold was designed to form the hollow during the TZCC process, as presented in Fig. 1(g).

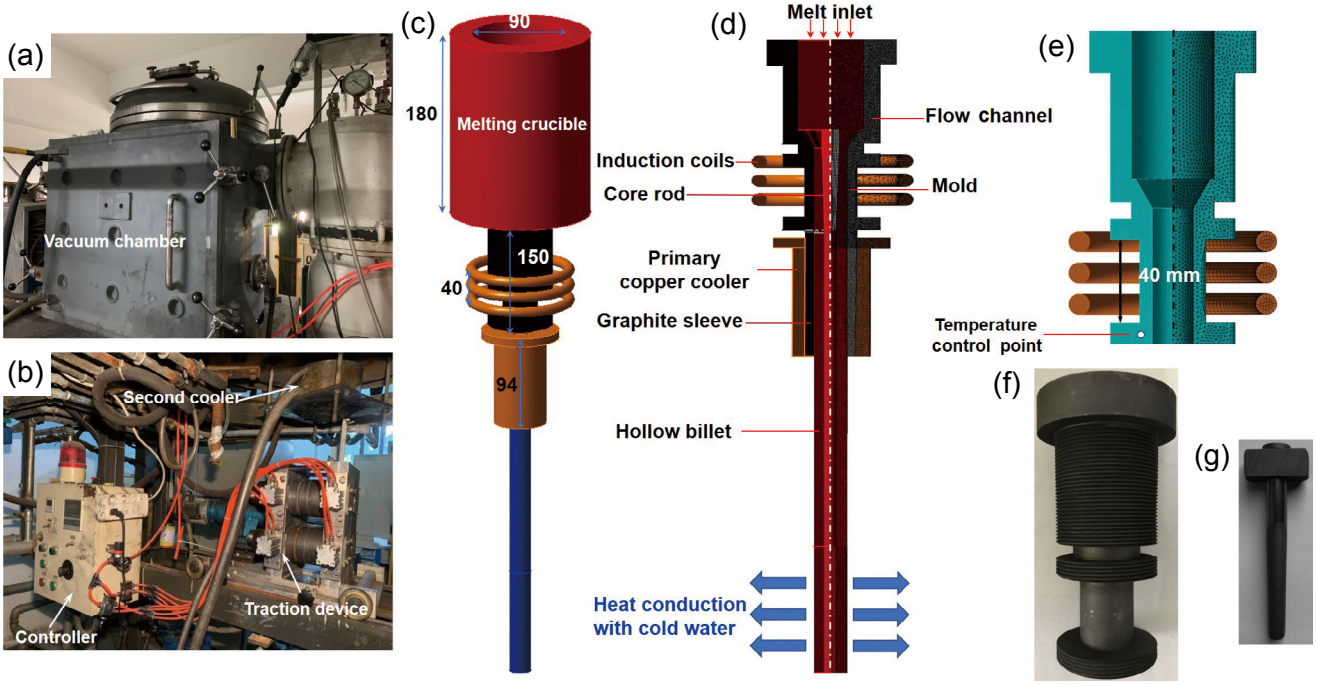

Fig. 1: Equipment and model of TZCC for preparing hollow billet: (a) and (b) equipment of TZCC; (c) simplified 3D model of TZCC; (d) mesh of TZCC; (e) and (f) model and real graphite flow channel and the mold; (g) graphite core rod

The equipment consists of a flow channel, mold, graphite core rod, induction heating coils, primary copper cooler, secondary cooler and dummy bar. The 2D12 aluminum alloy was melted in the crucible and flowed into the mold through the flow channel. After the melt filled the mold and contacted with the dummy bar, it was cooled by the primary copper cooler and the second cooler, which was below the mold. The thermophysical properties of the materials in the simulation are shown in Table 1 [17].

Table 1: Physical properties of materials for numerical analysis [17]

Physical properties	Coil (Copper)	Alloy (2D12)	Mold (Graphite)
Relative permeability	1	1	1
Resistivity (Ω·m)	1.67×10^{-8}	5.88×10^{-8}	1.00×10^{-5}
Permittivity	-	-	-
Density ($kg\cdot m^{-3}$)	8,940	2,750	2,250
Dynamic viscosity (Pa·s)	-	0.0013	-
Liquidus temperature (K)	-	920	-
Solidus temperature (K)	-	783	-
Latent heat ($J\cdot kg^{-1}$)	-	3.9×10^{5}	-
Thermal conductivity [$W\cdot(m\cdot K)^{-1}$]	260	95 (liquid)/180 (solid)	24
Specific heat capacity [$kJ\cdot(kg\cdot K)^{-1}$]	385	1,054 (liquid)/958 (solid)	710
Emissivity	0.3	0.3	0.85

2.2 Mathematical models, boundary conditions and numerical procedure

The temperature of the mold was controlled by the surrounding induction coils during the TZCC process. Furthermore, heat transfer between the mold and the melt changes the flow and temperature fields in the melt. A mushy zone forms due to intensive cooling by the primary cooler and secondary cooler, while downward pulling by the dummy bar leads to continuous solidification of the melt. Consequently, the combined effects of the electromagnetic field, flow field, temperature field and solidification (release of latent heat and influence on melt flow) during the TZCC process should be calculated. The governing equations of the mathematical models and the corresponding boundary conditions were reported in previous studies [18-20].

The 3D model was discretized using tetrahedral and hexahedral elements. There were 366,312 elements for solving the electromagnetic field using ANSYS, and 445,320 elements for solving the temperature field and flow field using Fluent. The electromagnetic field was first solved by using the finite element method, and then the Joule loss density and Lorenz force density were transferred into fluid dynamics differential equations via the source term and solved by using the finite volume method. A standard k-ε two-equation model with enhanced wall treatment was used to solve the turbulent flow, and a single Inter Xeon Gold 6254 processor of a Dell T7920 workstation was used to run the simulation.

2.3 Experimental procedure

In this experiment, a high-strength 2D12 aluminum alloy was used as a test material. The 2D12 aluminum alloy was firstly melted in the graphite crucible under an argon atmosphere in a vacuum chamber, and the temperature of the melt was kept at 1,003 K for 20 min. During TZCC, the stepped mold was inductively heated by coils, and the temperature at the temperature control point was measured by a tungsten-rhenium thermocouple and controlled by a proportion integration differentiation (PID) controller. The temperature of the mold was controlled at 853 K (the solidification interval of the 2D12 aluminum alloy is 783–920 K), and cooling water with a temperature of 295 K and flow rate of 400 $L\cdot h^{-1}$ passed through the primary cooling device. The melt flowed into the mold through the flow channel and connected with the dummy bar. Then, a hollow billet with an external diameter of 20 mm and an inner diameter of 5 mm was continuously fabricated by traction wheels at a speed of 2–6 $mm\cdot min^{-1}$. The surface quality of the hollow billets was photographed using a Canon EOS 800D Digital Single Lens Reflex camera. All samples were sectioned lengthways, and the microstructures were investigated by optical microscopy (OM), scanning electron microscopy (SEM) and energy-dispersive X-ray spectroscopy (EDS). The tensile tests were carried out on an MTS810 universal testing machine and the tensile speed was 1.0 $mm\cdot min^{-1}$.

3 Results and discussion

3.1 Numerical calculation of induction heating and model verification

The electromagnetic field was calculated, and the distribution of Joule loss density in the mold and Lorenz force density in

the melt is displayed in Fig. 2. The distribution of Joule loss density is not uniform along the axial and radial directions of the mold. The groove weakens the electromagnetic-thermal coupling as it is far from the coils, which leads to a lower Joule loss density in the grooves, while the maximum Joule loss density is located at the upper convex plate, as displayed in Fig. 2(a). Due to the electromagnetic shielding of the graphite mold, a stronger Lorenz force is generated in the groove of the mold at the middle of the coils, as shown in Fig. 2(b), and it points from the wall to the center, which is capable of inducing fluid flow in the melt.

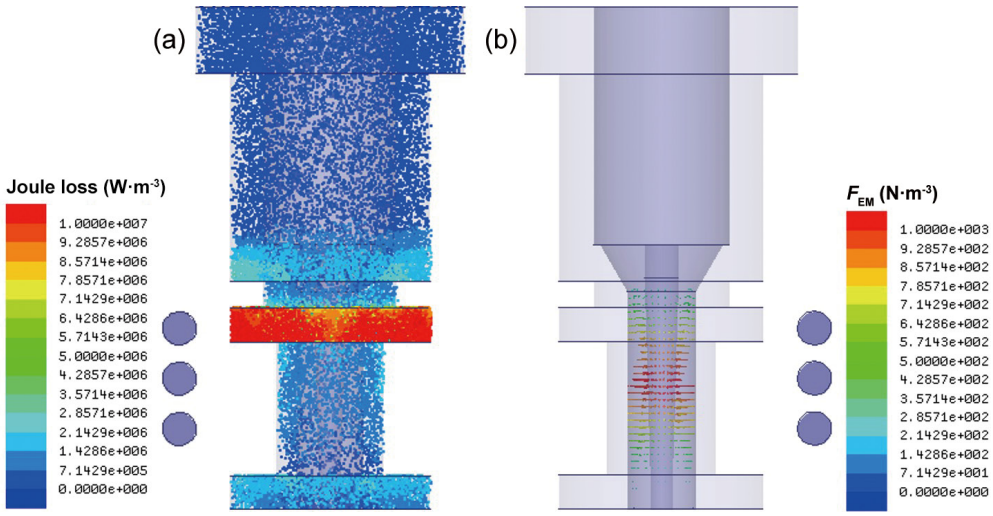

Fig. 2: Distribution of Joule loss density and Lorenz force density during TZCC: (a) Joule loss density in the mold; (b) Lorenz force density in the melt

The mold temperature during the induction heating process was measured and calculated to verify the accuracy of the 3D model, as shown in Fig. 3. The results show that the calculated and measured temperatures tend to reach the steady state at nearly 600 s and have similar value, which proves the accuracy of the model. The steady-state temperature field in the mold indicates that the highest temperature is in the upper convex plate, which is consistent with the distribution of Joule loss density. Moreover, intensive cooling below the mold leads to a vertical temperature gradient in the mold. Significantly different from the water-cooled mold used in traditional continuous casting, the induction heated stepped mold in TZCC can change the radial heat flux between the mold and melt, which affects the solidification process.

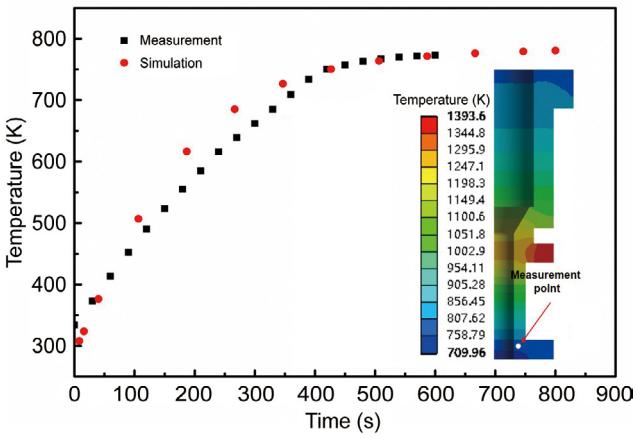

Fig. 3: Measurement and calculation of temperature in stepped diameter mold

3.2 Flow and temperature fields during TZCC

The temperature field and flow field during TZCC of 2D12 aluminum alloy hollow billets were calculated, and the distribution of liquid fraction, temperature and fluid flow at steady state is displayed in Fig. 4. The left sides of Fig. 4 present the liquid fractions in the core rod, melt and mold, while the right sides present the temperatures during solidification. A melt with a temperature of 1,003 K continuously flows into the mold through the flow channel, then radial and downward heat flux occur in the melt. A mushy zone with vertical temperature gradient forms between the core rod and mold during TZCC, where solid and liquid phases co-exist and columnar and equiaxed/globular grains develop. In the mushy zone, the growing crystals start to contact at the dendritic coherency point (DCP) and form a coherent dendritic network, which marks the boundary of the slurry zone and the porous zone and is defined as a solidification front [21]. The fluid flow ahead of the solidification front can transport the equiaxed/globular grains in the liquid, which strongly affects the solute distribution and macrosegregation during the solidification of the alloys [22]. In this study, the solid fraction at the DCP is approximately 10% for 2D12 aluminum alloy, which marks the solidification front, as shown in Fig. 4. As shown in the magnified images, a clockwise fluid flow forms ahead of the solidification front, which is the reverse of what occurs in direct-chill casting [9-11]. Melt flows downward along the inner wall of the hollow billet and then transversely from the inner wall to the outer wall ahead of the solidification front, finally in an upward direction and to the inner wall away from the solidification front, resulting in a circulation.

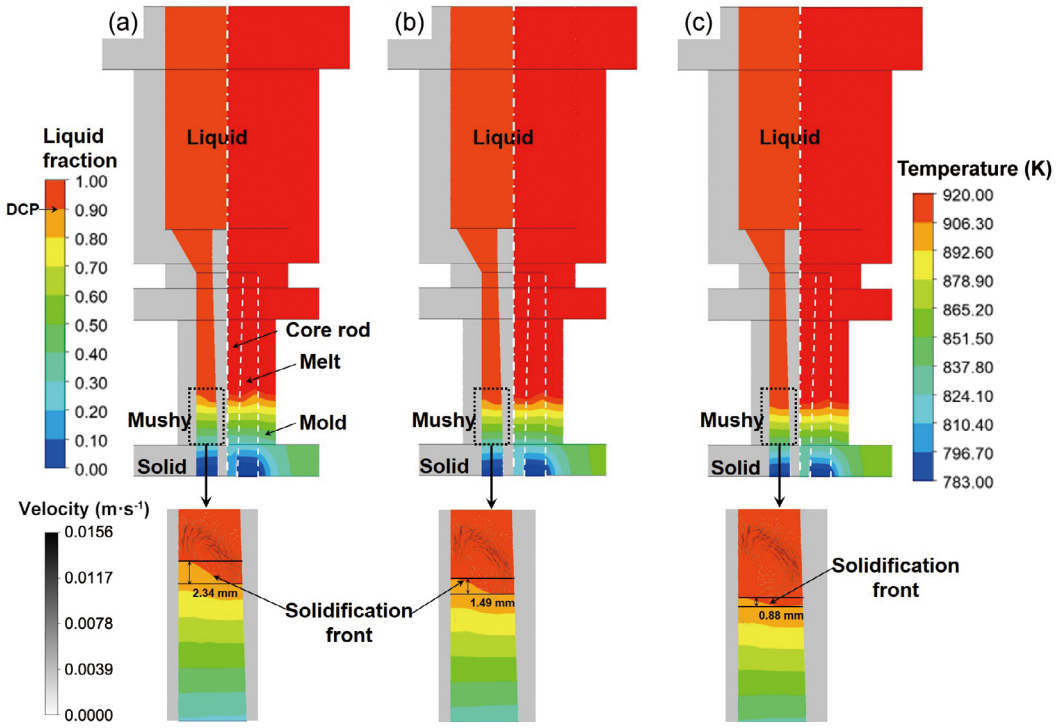

Fig. 4: Fluid flow, temperature and liquid fraction distribution of 2D12 aluminum alloy hollow billets by TZCC under different casting speeds: (a) 2 mm·min^{-1}; (b) 4 mm·min^{-1}; (c) 6 mm·min^{-1}

The heat flux is from the mold to the melt as the controlled mold temperature is higher than the solidus temperature of 2D12 aluminum alloy, and the convective heat transfer affects the deflection of the solidification front. The fluid flow transports the high-temperature melt from the outer wall to the inner wall, which results in a higher temperature in front of the solidification front. Consequently, the curved solidification front forms with a depressed region appearing near the inner wall and a protruding region appearing near the outer wall. The flux of melt increases under higher casting speed, which could increase the temperature of the melt in front of the mushy zone, while the temperature at the outlet of the mold is controlled constant. As a consequence, the solidification front moves downward and the height of the mushy zone decreases with increasing casting speed, and thus, the influence of the fluid flow on the deflection of the solidification front weakens. Therefore, the height difference of the solidification front is 2.34 mm at a casting speed of 2 mm·min^{-1} and decreases to 0.88 mm for a casting speed of 6 mm·min^{-1}, as displayed in Fig. 4.

Based on the calculated temperature field shown in Fig. 4, the average cooling rates in the typical temperature interval within the mushy zone for different casting speeds were calculated as the product of casting speed and temperature gradient, and are presented in Table 2. The temperature interval in Table 2 represents the formation of different intermetallics according to Shabestari et al [23]. It can be found the average cooling rate in the mushy zone increases with increasing casting speed, which can reduce segregation due to weakened solute redistribution under a higher cooling rate [21].

Table 2: Average cooling rate in typical temperature interval under different casting speeds

Casting speed (mm·min^{-1})	Average cooling rate (K·s^{-1})			
	920–783 K	894–881 K	836–810 K	783–743 K
2	0.21	0.21	0.20	0.21
4	0.41	0.41	0.39	0.43
6	0.61	0.63	0.61	0.65

During the TZCC process, the solute rejects at the solid-liquid interface due to solute redistribution accumulating in the vicinity of the solidification front. Additionally, the fluid flow transports the rejected solute in front of the mushy zone, coupled with the deflection of the solidification, finally would affect the macrosegregation. Under a lower casting speed, a stronger melt flow (from the outer wall to the inner wall) brings more solute to the inner wall of the hollow billet. The solute deposits in the depressed region, while a weaker transverse melt flow and the curved solidification front hinder the transportation of solute to the outer wall, which can result in the accumulation of solute near the inner wall of the hollow

billet. The clockwise fluid flow gradually moves away from the mushy zone and the deflection of the solidification front decreases with increasing casting speeds, which is beneficial in eliminating the macrosegregation during TZCC.

3.3 Characteristics of 2D12 aluminum alloy hollow billets prepared by TZCC

Based on the calculated results described above, 2D12 aluminum alloy hollow billets, shown in Fig. 5, were prepared by TZCC at casting speeds of 2, 4 and 6 mm·min^{-1}. As displayed in Figs. 5(a) and (b), hot tearing in the area marked by the red dotted box periodically appears on the hollow billets at casting speeds of 2 and 4 mm·min^{-1}, while the amount of hot tearing decreases with increasing casting speed, and even disappears at a casting speed of 6 mm·min^{-1}, as shown in Fig. 5(c). Additionally, the vertical section of the hollow billets in Fig. 5 shows that there are two kinds of hot tearing in the hollow billets: the upper hot tearing penetrates the hollow billet, while the lower hot tearing only appears near the inner wall of the hollow billet.

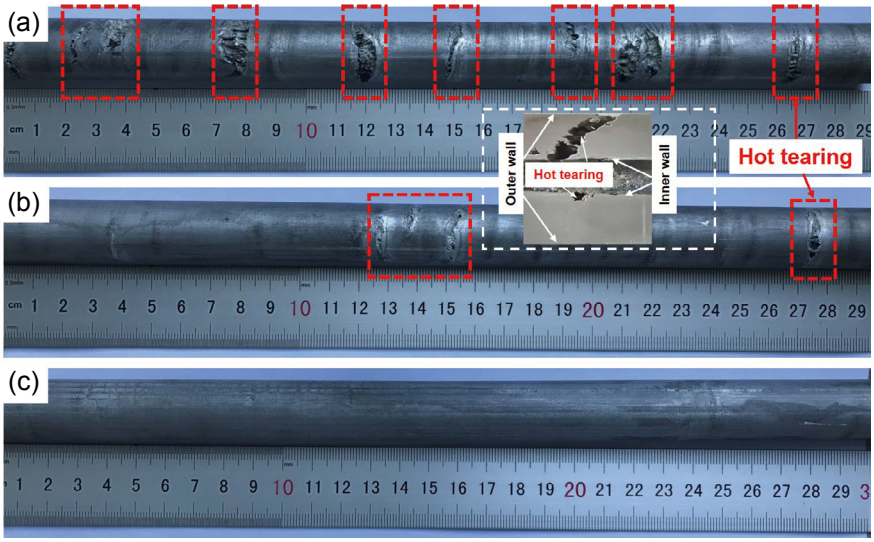

Fig. 5: 2D12 aluminum alloy hollow billets prepared by TZCC under different casting speeds: (a) 2 mm·min^{-1}; (b) 4 mm·min^{-1}; (c) 6 mm·min^{-1}

In order to reveal the formation and propagation mechanism of hot tearing, the vertical section of hollow billets was observed by OM and shown in Fig. 6. The left side of the images is the outer wall, while the right side of the images is the inner walls of the hollow billets. The hot tearing near the inner wall of hollow billets prepared at casting speeds of 2 and 4 mm·min^{-1} is displayed in Figs. 6(a) and (b). It is found that a hot tearing zone appears close to the inner walls of the hollow billets, and propagates to the outer walls of the hollow billets. However, no hot tearing is observed in Fig. 6(c) at a casting speed of 6 mm·min^{-1}. The hot tearing shown in Fig. 5 penetrates the hollow billets, while those in Fig. 6 do not penetrate the hollow billets.

The typical fracture morphologies (BSE and SE modes) in the hot tearing zone of the 2D12 aluminum alloy hollow billets at a casting speed of 2 mm·min^{-1} are shown in Fig. 7. Figures 7(a)–(d) present the typical morphologies in the hot tearing zone in the vertical section. Hot tearing appears in the α-Al matrix with blocky and dendritic morphology eutectic phases surrounding it, as displayed in Fig. 7(a). Pores emerge in the α-Al matrix accompanied by many bright dendritics, as shown in Fig. 7(b). The specific analysis of the phases was carried out by SEM and EDS later. Figures 7(c) and (d) show the fracture morphologies of the hot tearing, where dimples and eutectic phases can be observed. Below the rigidity temperature, the solid fraction increases and the dendritic network strengthens, while the concentration of alloying elements in the remaining liquid significantly increases and the melt permeability decreases [24]. Under this condition, hot tearing initiates in the porosity and propagates along the interdendritic and intergranular residual

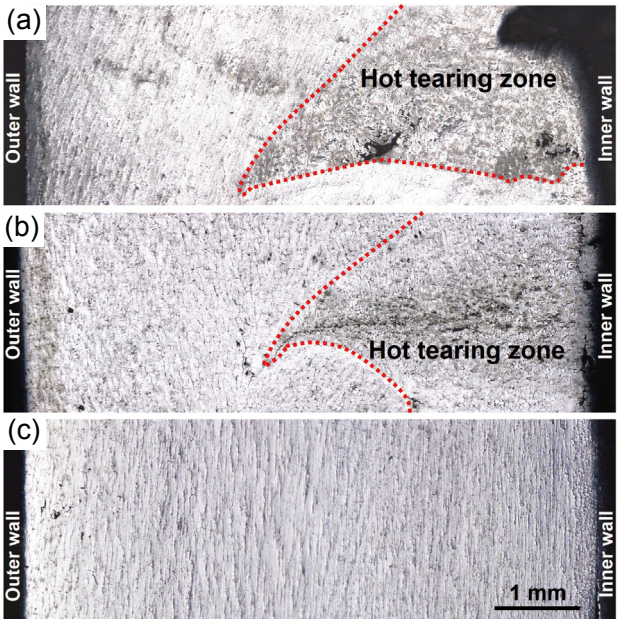

Fig. 6: Vertical section of 2D12 aluminum alloy hollow billets prepared by TZCC under different casting speeds: (a) 2 mm·min^{-1}; (b) 4 mm·min^{-1}; (c) 6 mm·min^{-1}

liquid, and even breaks through the dendritic network as the stress exceeds the network strength. As a consequence, dimples are found on the dendritic network, and eutectic phases appear at interdendritic and intergranular regions.

The hot tearing fracture morphologies at the cross section are displayed in Figs. 7(e) and (f), the fracture surfaces are significantly clean and smooth, and the grain boundary can be seen near the outer wall of the hollow billet in Fig. 7(e). The intergranular liquid films with liquid folds indicate that the intergranular residual liquid in the last stage of solidification connects the grains, while solidification shrinkage and insufficient liquid feeding result in fracture at lower casting speeds. Figure 7(f) shows the fracture surface near the inner wall of the hollow billet, which contains detached solid bridges and free dendritic structures. This indicates that hot tearing occurs through interdendritic separation of the liquid film in the mushy zone due to solidification shrinkage and insufficient liquid feeding.

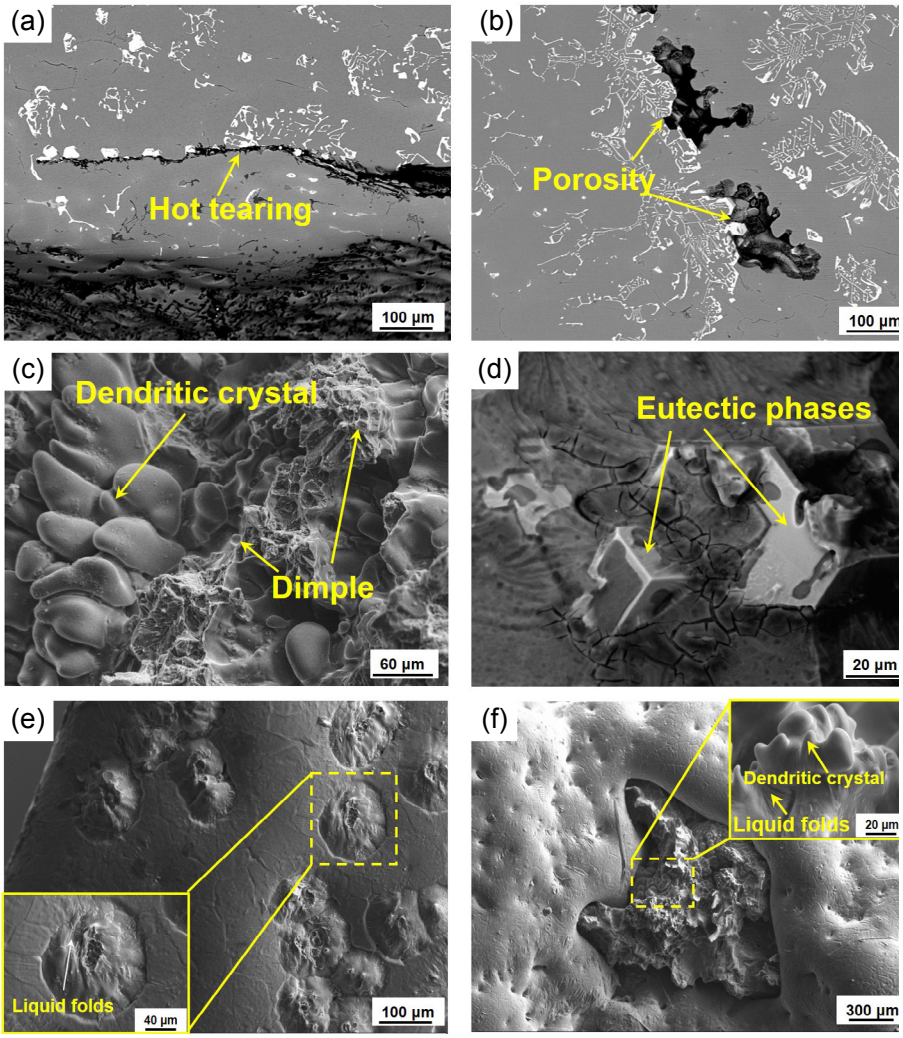

Fig. 7: Hot tearing fracture morphologies in hot tearing zone of 2D12 aluminum alloy hollow billet prepared by TZCC at a casting speed of 2 mm·min^{-1}: (a)–(d) vertical section; (e) and (f) cross section

The microstructures in the vertical section of the hollow billets at different casting speeds are displayed in Fig. 8. A mass of irregular eutectic phases concentrate near the inner wall of the hollow billet and form a macrosegregation band obviously separated from the α-Al matrix at casting speeds of 2 and 4 mm·min^{-1}, as displayed in Figs. 8(a) and (b). The widths of the bands decrease with increasing casting speed and even disappear at a casting speed of 6 mm·min^{-1}, as shown in Fig. 8(c). The microstructures of the high-strength aluminum alloys prepared by TZCC are obviously different from those prepared by direct-chill casting due to the temperature of the mold [11]. The average content of solute elements in Fig. 8 was tested by EDS, and the total weight percentage of solute elements from the inner wall to the outer wall is, 5.73wt.%, 2.14wt.% and 1.70wt.% at a casting speed of 2 mm·min^{-1}, 4.55wt.%, 2.26wt.% and 1.41wt.% at a casting speed of 4 mm·min^{-1}, and 2.13wt.%, 2.37wt.% and 2.29wt.% at a casting speed of 6 mm·min^{-1}. Results indicate that the higher average content of solute elements appears near the inner wall while lower average content of solute elements appears near the outer wall of the hollow billet at a casting speed of 2 and 4 mm·min^{-1}. However, it is uniformly distributed at a casting speed of 6 mm·min^{-1}.

The specific micrographs of the bright phases at a casting speed of 2 mm·min^{-1} were generated using a SEM in the BSE mode, and the compositions were determined by EDS, as displayed in Fig. 9. As the partition coefficients of solute Cu,

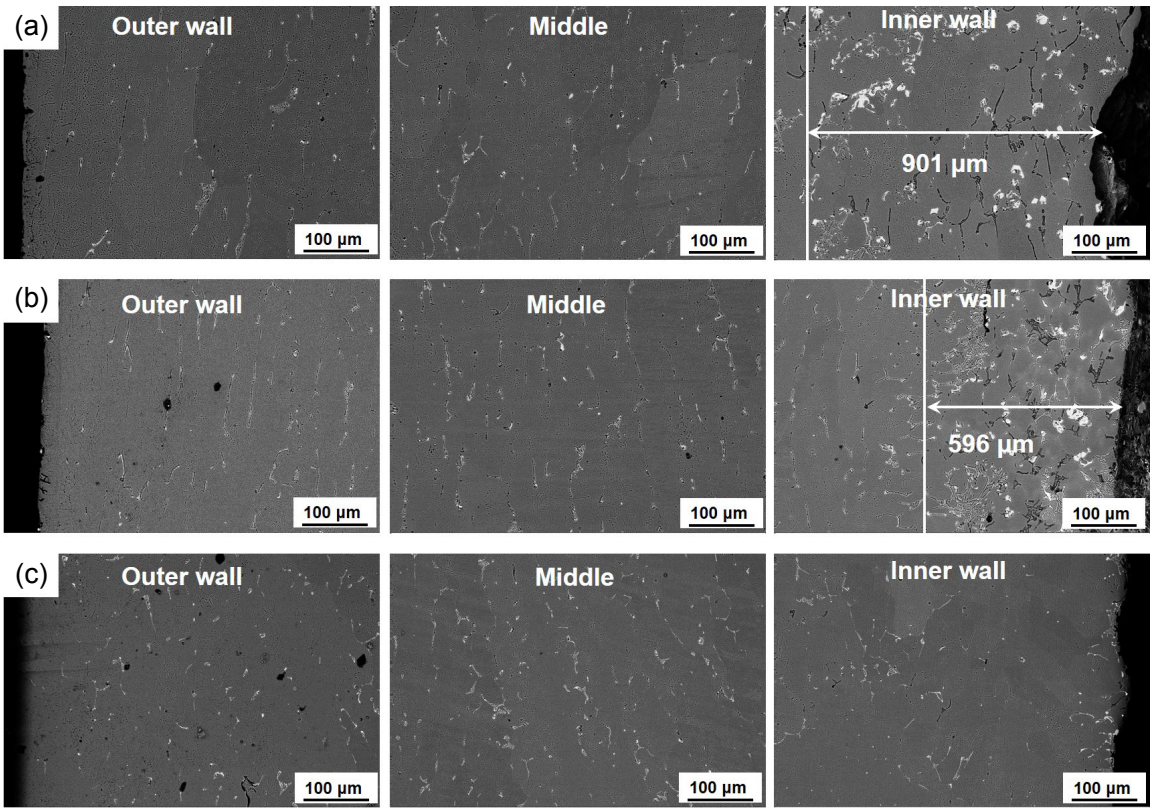

Fig. 8: Microstructure characteristics in 2D12 aluminum alloy hollow billets prepared by TZCC under different casting speeds: (a) 2 mm·min^{-1}; (b) 4 mm·min^{-1}; (c) 6 mm·min^{-1}

Mg, Si and Fe are much less than 1, stronger partitioning of those alloying elements occurs during the continuous casting process [25]. The EDS maps of the elemental distributions indicate that the eutectic phases are rich in element Cu, Mg, Si, Fe and Mn, and are transformed from the intergranular residual liquid in the last stage of solidification due to stronger redistribution of solute under a lower cooling rate. EDS analysis of the eutectic phases and matrix (Point 5) were conducted, and the results are shown in Table 3. Points 1 to 4 indicate that the eutectic phases are intermetallics consisting of $Al_{15}(CuFeMn)_3Si_2$, $Al_{20}Cu_2Mn_3$, Al_2Cu and Mg_2Si.

According to the microstructure characteristics of the hollow billets, the solute segregation gradually reduces with increasing casting speed, which decreases the residual liquid in the last solidification stage and hinders the initiation and propagation of hot tearing. At casting speeds of 2 mm·min^{-1} and 4 mm·min^{-1}, the solute transfer ahead of the solidification front and lower cooling rate result in the accumulation of solute near the inner walls of the hollow billets. The accumulated solute in the melt decreases the solidification temperature and forms interdendritic and intergranular liquid films in the last stage of solidification within the mushy

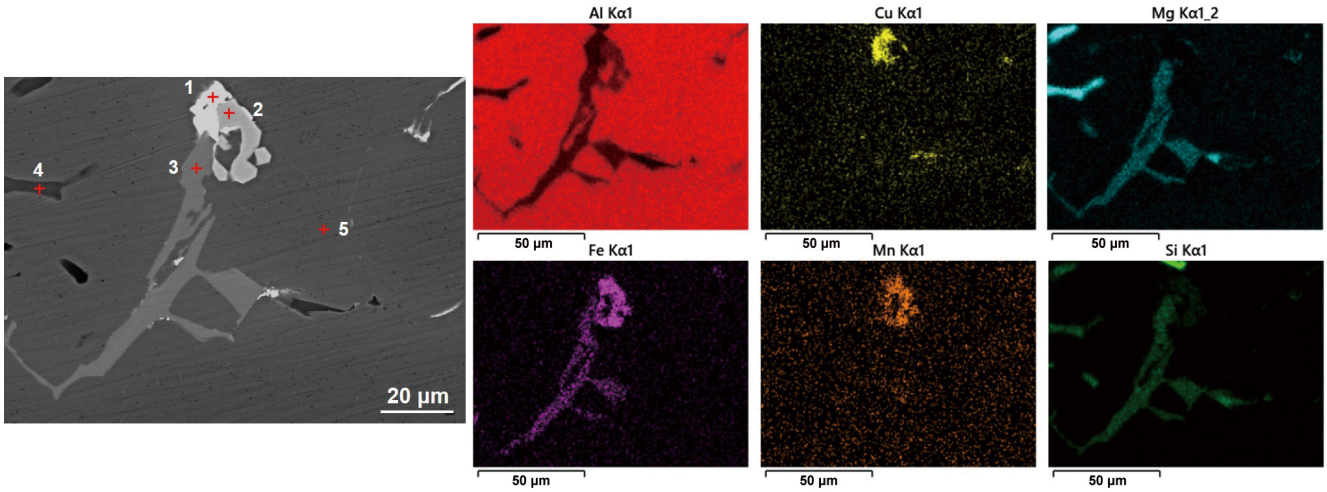

Fig. 9: Microstructure and EDS maps of elemental distribution in 2D12 aluminum alloy hollow billet prepared by TZCC at a casting speed of 2 mm·min^{-1}

Table 3: EDS results of intermetallic phases and matrix observed in Fig. 9 (wt.%)

Elements	Point 1	Point 2	Point 3	Point 4	Point 5
Al	43.99	56.69	46.63	26.22	97.60
Cu	54.84	1.96	0.26	0.15	0.99
Mg	0.12	0.19	16.51	45.74	0.30
Mn	0.07	8.08	0.73	0.07	0.10
Fe	0.58	20.71	9.14	0.00	0.00
Si	0.39	9.37	26.73	27.82	1.01

zone. Near the end of solidification (when the solid fraction approaches 1), micropores emerge in the residual liquid due to solidification shrinkage, thermal stress is induced by thermal contraction, and the hot tearing initiates and is propagated through the interdendritic structure. However, a relatively flat solidification front and higher cooling rate at a casting speed of 6 mm·min^{-1} decrease the residual liquid in the last solidification stage, which in turn weakens the solidification shrinkage and insufficient liquid feeding, and thus eliminating the macrosegregation and hindering the initiation and propagation of hot tearing.

The microstructures of the vertical sections of the hollow billets at different casting speeds are displayed in Fig. 10. Columnar crystals nearly parallel to the casting direction form in the hollow billets due to the vertical temperature gradient during solidification, and the average size of columnar crystals decreases from 87.64 mm to 53.02 mm with increasing casting speed. Moreover, larger irregular eutectic phases appear in the intergranular zone of the columnar crystals, smaller dotted eutectic phases emerge in the intragranular, and the quantities of the eutectic phases decrease with an increase of casting speed. The room temperature tensile properties of 2D12 aluminum alloy hollow billets prepared by TZCC at casting speeds of 4 mm·min^{-1} and 6 mm·min^{-1} were tested, and the engineering stress-strain curves are shown in Fig. 11. The average tensile strength and elongation after fracture are 209 MPa and 20% at a casting speed of 6 mm·min^{-1}, respectively, and are higher than that of at a casting speed of 4 mm·min^{-1}. The 2D12 aluminum alloy hollow billets prepared by TZCC eliminate the hot tearing and macrosegregation defects, and have the finest

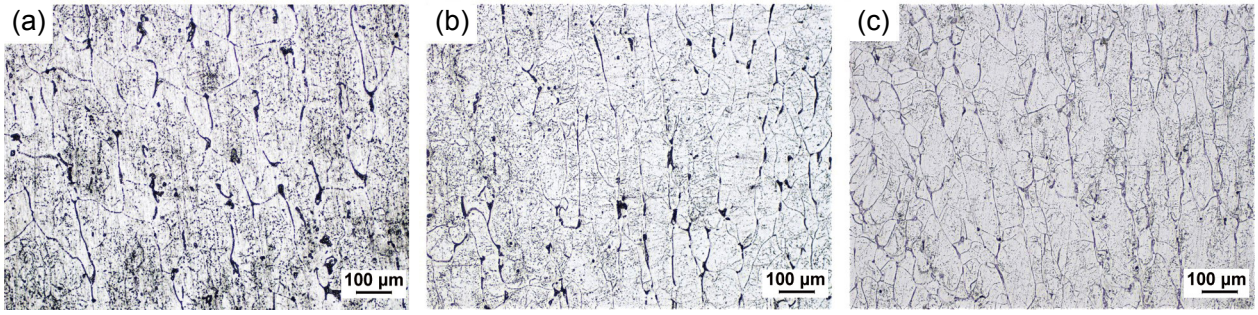

Fig. 10: Microstructures of 2D12 aluminum alloy hollow billets prepared by TZCC under different casting speeds: (a) 2 mm·min^{-1}; (b) 4 mm·min^{-1}; (c) 6 mm·min^{-1}

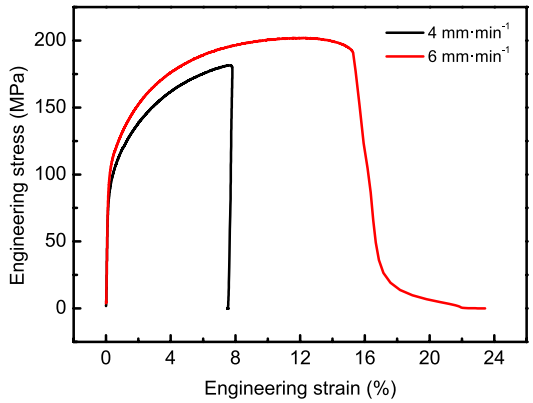

Fig. 11: Engineering stress-strain curves of 2D12 aluminum alloy hollow billets prepared by TZCC under different casting speeds

columnar crystals and reduced brittle intermetallic phases at a casting speed of 6 mm·min^{-1}. These excellent mechanical properties are beneficial for further plastic forming processes.

4 Conclusions

(1) The flow and temperature fields during TZCC were calculated by a verified 3D model at casting speeds of 2, 4, and 6 mm·min^{-1}. The results indicate that a circular fluid flow appears ahead of the solidification front and that a vertical temperature gradient forms in the mushy zone.

(2) The induction heated mold and the convective heat transfer lead to a curved solidification front, and a depressed region appears near the inner wall of the hollow billet. The deflection of the solidification front decreases and the average

cooling rate in the mushy zone increases with increasing casting speed.

(3) Hot tearing periodically appears in the hollow billets accompanied by macrosegregation near the inner wall at casting speeds of 2 and 4 mm·min^{-1}, while the amount of hot tearing decreases with increasing casting speed. A relatively flat solidification front and higher cooling rate at a casting speed of 6 mm·min^{-1} decrease the residual liquid in the last solidification stage and thus eliminate the macrosegregation and hinder the initiation and propagation of hot tearing.

(4) 2D12 aluminum alloy hollow billet with eliminated macroscopic defects of macrosegregation and hot tearing, and the finest columnar crystals can be prepared by TZCC at a casting speed of 6 mm·min^{-1}. Its tensile strength and elongation reach 209 MPa and 20%, respectively, which are beneficial for the further plastic forming process.

Acknowledgements

This work was supported by the National Natural Science Foundation of China (No. U1703131, No. 51674027, No. 51974027 and No. 52004028), Guangdong Basic and Applied Basic Research Foundation (2019A1515111126) and the Fundamental Research Funds for the Central Universities (FRF-TP-18-005C1 and FRF-TP-18-041A1).

References

[1] Liu N, Jie J C, Lu Y P, et al. Characteristics of clad aluminum hollow billet prepared by horizontal continuous casting. J. Mater. Process. Technol., 2014, 214(1): 60–66.
[2] Liu X, Xu J X, Zhao F, et al. Effect of homogenization on second phases and mechanical properties of AA 5052 aluminum alloy tube billets fabricated by HCCM vertical continuous casting. J. Alloy. Compd., 2022, 901: 163645.
[3] Li H, Wei D, Zhang H Q, et al. Texture evolution and controlling of high-strength titanium alloy tube in cold pilgering for properties tailoring. J. Mater. Process. Technol., 2020, 279: 116520.
[4] Zhang Z, Liu D, Zhang R Q, et al. Experimental and numerical analysis of rotary tube piercing process for producing thick-walled tubes of nickel-base superalloy. J. Mater. Process. Technol., 2020, 279: 116557.
[5] Hussain S, Cui C S, He L, et al. Effect of hot gas atomization on spray forming of steel tubes using a close-coupled atomizer (CCA). J. Mater. Process. Technol., 2020, 282: 116677.
[6] Fu H G, Xiao Q, Xing J D. A study of segregation mechanism in centrifugal cast high speed steel rolls. Mater. Sci. Eng. A, 2008, 479(1–2): 253–260.
[7] Yan G J, Xu Y, Jiang B L. The production of high-density hollow cast-iron bars by vertically continuous casting. J. Mater. Process. Technol., 2012, 212(1): 15–18.
[8] Du Q, Eskin D G, Katgerman L. Modeling macrosegregation during direct-chill casting of multicomponent aluminum alloys. Metall. Mater. Trans. A, 2007, 38(1): 180–189.
[9] Guan R, Ji C, Wu C H, et al. Numerical modelling of fluid flow and macrosegregation in a continuous casting slab with asymmetrical bulging and mechanical reduction. Int. J. Heat Mass Transfer, 2019, 141: 503–516.
[10] Ohno M, Sato H. Macrosegregation simulation model based on Lattice-Boltzmann method with high computational efficiency. Int. J. Heat Mass Transfer, 2018, 127B: 561–570.
[11] Luo H J, Jie W Q, Gao Z M, et al. Numerical simulation for macrosegregation in direct-chill casting of 2024 aluminum alloy with an extended continuum mixture model. Trans. Nonferrous Met. Soc. China, 2018, 28(5): 1007–1015.
[12] Paramatmuni R K, Chang K M, Kang B S, et al. Evaluation of cracking resistance of DC casting high strength aluminum ingots. Mater. Sci. Eng. A, 2004, 379(1–2): 293–301.
[13] Bai Q L, Liu J C, Li H X, et al. A modified hot tearing criterion for direct chill casting of aluminium alloys. Mater. Sci. Tech., 2016, 32(8): 846–854.
[14] Mathier V, Vernède S, Jarry P, et al. Two-phase modeling of hot tearing in aluminum alloys: Applications of a semicoupled method. Metall. Mater. Trans. A, 2009, 40: 943.
[15] Suyitno, Savran V I, Katgerman L, et al. Effects of alloy composition and casting speed on structure formation and hot tearing during direct-chill casting of Al-Cu alloys. Metall. Mater. Trans. A, 2004, 35: 3551–3561.
[16] Liu X F, Luo J H, Wang X C, et al. Casting device and method with solid-liquid phase area temperature as mold temperature. China Patent No. WO2011127785, 2011-10-20.
[17] Yang Y H, Liu X F, Wang S Q. Thermal characteristics of induction heating with stepped diameter mold during two-phase zone continuous casting high-strength aluminum alloys. Int. J. Heat Mass Transfer, 2020, 152: 119479.
[18] Lu L L, Zhang S M, Xu J, et al. Numerical study of titanium melting by high frequency inductive heating. Int. J. Heat Mass Transfer, 2017, 108B: 2021–2028.
[19] Liu W W, Feng Y F, Sun J N, et al. Analysis of the thermal-mechanical problem in the process of flexible roll profile electromagnetic control. Int. J. Heat Mass Transfer, 2018, 120: 447–457.
[20] Liu X F, Liao W N, Yang Y H. Thermal characteristics and uniformity of microstructures during temperature controlled mold continuous casting profiled copper alloy strip. Int. Commun. Heat Mass Transfer, 2020, 110: 104414.
[21] Ghoncheh M H, Shabestari S G. Effect of cooling rate on the dendrite coherency point during solidification of Al2024 alloy. Metall. Mater. Trans. A, 2015, 464: 1287–1299.
[22] Seredyński M, Banaszek J. Coupled enthalpy-porosity and front tracking approach to modeling chemical inhomogeneity in solidifying metal alloys. Int. J. Heat Mass Transfer, 2021, 173: 121221.
[23] Shabestari S G, Ghoncheh M H, Momeni H. Evaluation of formation of intermetallic compounds in Al2024 alloy using thermal analysis technique. Thermochim. Acta, 2014, 589: 174–182.
[24] Djurdjevic M B, Huber G. Determination of rigidity point/temperature using thermal analysis method and mechanical technique. J. Alloy. Compd., 2014, 590: 500–506.
[25] Nadella R, Eskin D G, Du Q, et al. Macrosegregation in direct-chill casting of aluminium alloys. Prog. Mater. Sci., 2008, 53(3): 421–480.